CSMA 2024
16ème Colloque National en Calcul des Structures
13-17 Mai 2024, Presqu'île de Giens (Var)

Numerical analysis of an enriched beam model

M. SHARIFI[1], F. DAUDE[1,2], C. STOLZ[1]

[1],*IMSIA, UMR EDF-CNRS-CEA-ENSTA 9219, F-91762 Palaiseau, France mahshid-externe.sharifi@edf.fr*
[2] *EDF Lab Paris-Saclay, R&D, 7 Boulevard Gaspard Monge 91120 Palaiseau, France*

Abstract — The finite element for a thin-walled tube developped in [1] is considered. A classical Euler-Bernoulli beam element has been enriched in order to take into account the influence of the rotations of the mid-surface on the local deformations of the tube cross-sections. The latter is a semi-analytical model using a Fourier expansion based on the circumferential variable. A grid convergence study of the enriched model is carried out for different mesh discretisations. Next, the stability of the explicit time integration is studied using the lumped mass matrix and the critical time steps associated to the mass matrix lumping are estimated.
Mots clés — Finite Element Method, Enriched Model, Stability Condition.

1 Introduction

Modelling of piping systems has become of a high importance in recent decades due to their wide use in industry. Various numerical models have been employed to study the dynamic behavior of pipelines but most studies are limited to either a beam or a shell model. The classical beam model does not allow the variations of the tube cross-section which have been proved to present significant deformations under bending [3]. On the other hand, the shell models are capable of presenting the evolution of the tube cross-section but lead to a high computational cost. As a result, computationally efficient models have been developed allowing to take into account the variations of the tube cross-section as the hybrid shell-beam model proposed in [1]. A thorough review of such models can be found in [4]. In extension to the work presented in [1], further improvements on this hybrid shell-beam model are here achieved while a special attention is given to its computational efficiency. As in [1], an explicit time integration is employed where the mass matrix is replaced by a lumped mass matrix in order to enhance the computational cost of the numerical scheme. To further improve the latter, the impact of the rotational terms of the lumped mass matrix on the critical time step value is analysed.

Five main sections are defined in this paper. First section briefly represents the theoretical model. The second section details the numerical explicit finite-element solver and the corresponding lumped matrix. The third section demonstrates the dependancy of the stability of the numerical scheme to the coefficients of the rotational terms. The fourth section presents some of the results concerning a mesh convergence and the study of the numerical stability. Finally, the last section draws some conclusions over the presented work and a few perspectives.

2 Theoretical tube model

The model has been presented in details in [1]. A straight tube presented in figure 1, with a length L, mean radius a and thickness e is considered. The kinematics of the tube are expressed by the classical Eurler-Bernoulli beam theory enriched by a Kirchhoff-Love shell model. The beam motions are expressed in the $(\mathbf{E_x},\mathbf{E_y},\mathbf{E_z})$ basis using the displacements $U_0(t,x)$, $W_0(t,x)$, $V_0(t,x)$ and rotations $\Omega_x(t,x)$, $\Omega_y(t,x)$, $\Omega_z(t,x)$ with respect to each axis. Displacements of the cross-section associated to the shell kinematics are expressed in the $(\mathbf{E_x},\mathbf{E_r},\mathbf{E_\theta})$ frame by $u(t,x,\theta,z)$, $w(t,x,\theta,z)$, $v(t,x,\theta,z)$, where t denotes the time. It needs to be noted that the variation along $\mathbf{E_r}$ is considered as $\frac{-e}{2} < z < \frac{e}{2}$.

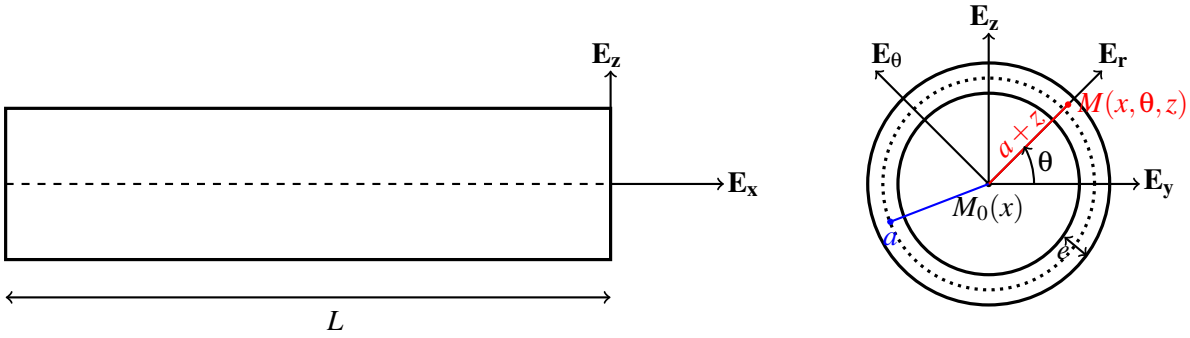

Figure 1: The scheme of the tube, the side view (on the left), the cross-section view (on the right)

The coordinates of the point $\mathbf{M}(x,\theta,z)$ in the initial state can be expressed using the point on the neutral axis $M_0(x)$:

$$\mathbf{M}(x,\theta,z) = \mathbf{M_0}(x) + (a+z)\mathbf{E_r} = x\mathbf{E_x} + (a+z)\mathbf{E_r} \tag{1}$$

The coordinates of the point $\mathbf{m}(x,\theta,z)$ in the deformed state using equation (1) reads:

$$\begin{aligned}&\mathbf{m}(x,\theta,z) = \mathbf{M}(x,\theta,z) + \mathbf{U} = \\ &x\mathbf{E_x} + (a+z)\mathbf{E_r} + U_0\mathbf{E_x} + W_0\mathbf{E_y} + V_0\mathbf{E_z} + u\mathbf{E_x} + w\mathbf{E_r} + v\mathbf{E_\theta} + \\ &(\Omega_x\mathbf{E_x} + \Omega_y\mathbf{E_y} + \Omega_z\mathbf{E_z}) \wedge (u\mathbf{E_x} + (a+z+w)\mathbf{E_r} + v\mathbf{E_\theta})\end{aligned} \tag{2}$$

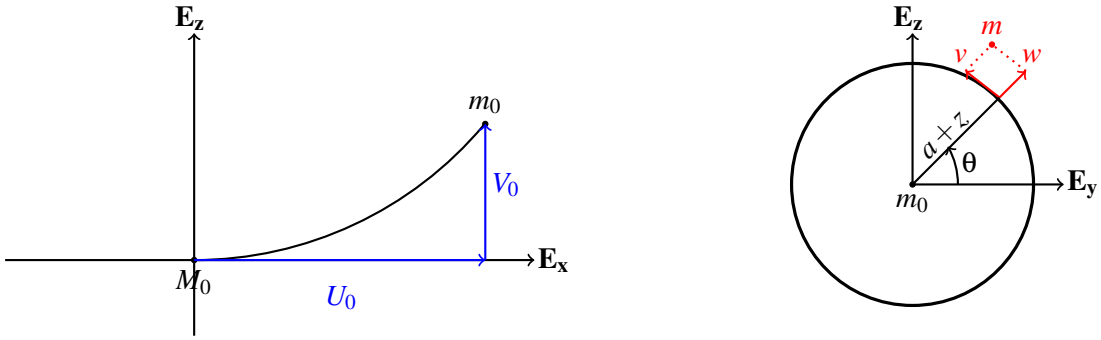

Figure 2: The deformed tube, beam model (on the left), the shell cross-section (on the right)

The coordinates of the point in the deformed state can be expressed in the cylindrical basis ($\mathbf{E_x}$,$\mathbf{E_r}$,$\mathbf{E_\theta}$):

$$\begin{aligned}\mathbf{m}(x,\theta,z) =& (x + U_0 + u + (a+z)\sin\theta\Omega_y - (a+z)\cos\theta\Omega_z)\mathbf{E_x} + \\ &(a+z+w+W_0\cos\theta + V_0\sin\theta)\mathbf{E_r} + \\ &(v + V_0\cos\theta - W_0\sin\theta + (a+z)\Omega_x)\mathbf{E_\theta}\end{aligned} \tag{3}$$

In (3) the non-linear terms of displacements have been neglected but are detailed in [1].

As a result of the first-order shear deformation shell theory, the displacement field reads:

$$w = w_0, \quad v = v_0 + zv_1, \quad u = u_0 - zu_1$$

with u_1 and v_1 the rotation angles of the mid-surface of transverse normal $\mathbf{E_r}$ in the ($\mathbf{E_x}$, $\mathbf{E_r}$) and ($\mathbf{E_r}$, $\mathbf{E_\theta}$) planes, respectively.

Due to the thin-shell hypothesis, the term $\dfrac{1}{a+z}$ can be approximated as:

$$\frac{1}{a+z} = \frac{1}{a} - \frac{z}{a^2} + o\left(\frac{z}{a^2}\right)$$

Finally, using the displacements expressed in equation (3), the Euler-Bernoulli condition for the beam contributions and the Kirchhoff-Love Theory for the shell contributions, the strain tensor is obtained [1]. The strain tensor is a sum of membrane term, ε^m and a linear term in z representing the local curvature $\mathbf{k}$, $\varepsilon = \varepsilon^m + z\mathbf{k}$.

$$\begin{cases} \varepsilon^m_{xx} = \dfrac{\partial U_o}{\partial x} - a\sin\theta\dfrac{\partial^2 V_0}{\partial x^2} - a\cos\theta\dfrac{\partial^2 W_0}{\partial x^2} + \dfrac{\partial u_0}{\partial x} \\ \varepsilon^m_{\theta\theta} = \dfrac{1}{a}\left(\dfrac{\partial v_0}{\partial\theta} + w_0\right) \\ 2\varepsilon^m_{x\theta} = \dfrac{1}{a}\dfrac{\partial u_0}{\partial\theta} + \dfrac{\partial v_0}{\partial x} + a\dfrac{\partial\Omega_x}{\partial x} \\ k_{xx} = -\sin\theta\dfrac{\partial^2 V_0}{\partial x^2} - \cos\theta\dfrac{\partial^2 W_0}{\partial x^2} - \dfrac{\partial^2 w_0}{\partial x^2} \\ k_{\theta\theta} = -\dfrac{1}{a^2}\left(\dfrac{\partial^2 w_0}{\partial\theta^2} + w_0\right) \\ 2k_{x\theta} = -\dfrac{1}{a}(2\dfrac{\partial^2 w_0}{\partial x\partial\theta} + \dfrac{1}{a}\dfrac{\partial u_0}{\partial\theta} - \dfrac{\partial v_0}{\partial x}) + \dfrac{\partial\Omega_x}{\partial x} \end{cases}$$

The constraint tensor can thus be expressed using the strain tensor, the Young modulus, E and the Poisson coefficient ν:

$$\begin{cases} \sigma = \sigma^m + z\sigma^k \\ \sigma = \dfrac{E}{1-\nu}\left((1-\nu)\varepsilon + \nu\,\mathrm{trac}(\varepsilon)\,\mathbf{I}\right) \end{cases}$$

A Fourier expansion is employed to express the shell displacement field in terms of the tangential variable θ. It needs to be noted that the rigid-body motions in the shell kinematics are set equal to zero in order to avoid any redundancy with the beam body motion ($u^c_o = 0$, $u^c_1 = 0$, $u^s_1 = 0$, $v^c_0 = 0$). In addition, $v^c_1 = -w^s_1$ and $v^s_1 = w^c_1$ to produce a vanishing rigid-body displacement of the cross-section in the $\mathbf{E_z}$ and $\mathbf{E_y}$ directions, respectively. Moreover, an inextensibility condition is taken into account ($\varepsilon^m_{\theta\theta} = 0$ for $i \geq 2$ Fourier modes greater than 2).

Finally, the Fourier expansion of the shell displacements reads:

$$\begin{cases} u_o(t,x,\theta) = & & \displaystyle\sum_{i=2}^{N_f}\left(u^c_i(t,x)\cos(i\theta) + u^s_i(t,x)\sin(i\theta)\right) \\ v_o(t,x,\theta) = & -w^s_1(t,x)\cos\theta + w^c_1(t,x)\sin\theta + & \displaystyle\sum_{i=2}^{N_f}\left(\frac{1}{i}w^s_i(t,x)\cos(i\theta) - \frac{1}{i}w^c_i(t,x)\sin(i\theta)\right) \\ w_o(t,x,\theta) = w^c_o(t,x) & +w^c_1(t,x)\cos\theta + w^s_1(t,x)\sin\theta + & \displaystyle\sum_{i=2}^{N_f}\left(w^c_i(t,x)\cos(i\theta) + w^s_i(t,x)\sin(i\theta)\right) \end{cases}$$

where N_f represents the number of Fourier modes considered in the expansion. The index c and s represent the coefficients in cosine and sine of the Fourier expansion, respectively.

As a results of this expansion, the Kirchhoff-Love conditions are expressed as:

$$u_1 = \frac{\partial w_o}{\partial x} \quad \text{and} \quad v_1 = -\frac{1}{a}\left(2w^s_1\cos\theta - 2w^c_1\sin\theta + \sum_{i=2}^{N_f}\frac{i^2-1}{i}\left(w^s_i\cos(i\theta) - w^c_i\sin(i\theta)\right)\right)$$

Finally, the virtual power principle is employed to obtain the tube equation of motion:

$$\mathcal{P}_a = \mathcal{P}_e + \mathcal{P}_i$$

with $\mathcal{P}_a$, $\mathcal{P}_e$ and $\mathcal{P}_i$ the power of inertia, external and internal forces, respectively.

Each of the powers can be written using the elements defined previously:

$$\mathcal{P}_a = \int_\Omega \rho \frac{\partial^2 \mathbf{U}}{\partial t^2} . \delta\mathbf{U}\, dV \qquad \mathcal{P}_e = \int_{\delta\Omega} \mathbf{T} . \delta\mathbf{U}\, dS \qquad \mathcal{P}_i = -\int_\Omega \sigma : \delta\varepsilon\, dV$$

where ρ is the solid density, Ω the current volume, $\frac{\partial^2 \mathbf{U}}{\partial t^2}$ the acceleration vector, $\delta\mathbf{U}$ the virtual displacement, $\mathbf{T}$ the vector of applied forces on the boundaries, σ the Cauchy stress tensor and $\delta\varepsilon$ the virtual strain tensor.

3 Numerical Solver

The Finite Element Method (FEM) has been employed to approximate the equation of motion expressed in the previous section. For this purpose, the tube model has been discretised in multiple elements of equal size, ℓ_e. The displacement field is approximated over each element using shape functions which are considered as linear for the displacements along $\mathbf{E_x}$ (for both beam and shell contributions) and cubic for the other degrees of freedom:

$$\mathbf{d_e} = (U_0, W_0, V_0, \Omega_x, \Omega_z, \Omega_y, w_0^c, u_1, w_1^s, dw_1^s, u_2^c, du_2^c, w_2^c, dw_2^c, \ldots)$$

The shape function tensor for each element (subscribe e) contains the tensors corresponding to nodes at each end of the element:

$$\mathbf{N}_e = \left(\mathbf{N}_e^1\, \mathbf{N}_e^2\right)$$

Using the definition of the power of inertia and the approximation of the displacement field by the shape functions, the consistent mass matrix can be evaluated:

$$\mathbf{M}_e = \begin{pmatrix} \mathbf{M}_e^{11} & \mathbf{M}_e^{12} \\ \mathbf{M}_e^{21} & \mathbf{M}_e^{22} \end{pmatrix} \quad \text{with} \quad \mathbf{M}_e^{ij} = \int_{V_e} \rho \left(\mathbf{N}_e^i\right)^T \mathbf{T}^T \mathbf{T} \mathbf{N}_e^j\, dV$$

Each sub-matrix ($\mathbf{M}_e^{11}$,$\mathbf{M}_e^{22}$,$\mathbf{M}_e^{12}$) has a beam (b) and a shell (s) contribution. The non-diagonal terms are denoted as (bs) and the number specifying the Fourier mode of the shell degree of freedom. Matrix $\mathbf{M}_e^{11}$ is thus expressed as:

$$\mathbf{M}_e^{11} = \begin{pmatrix} \mathbf{M}_e^{11,b} & 0 & \mathbf{M}_e^{11,bs_1} & 0 & \cdots & 0 \\ 0 & \mathbf{M}_e^{11,s_0} & 0 & 0 & \cdots & 0 \\ (\mathbf{M}_e^{11,bs_1})^T & 0 & \mathbf{M}_e^{11,s_1} & 0 & \cdots & 0 \\ 0 & 0 & 0 & \mathbf{M}_e^{11,s_2} & \cdots & 0 \\ \vdots & \vdots & \vdots & \vdots & \ddots & \vdots \\ 0 & 0 & 0 & 0 & \cdots & \mathbf{M}_e^{11,s_i} \end{pmatrix}$$

$$\mathbf{M}_e^{11,b} = \rho S \ell_e \begin{pmatrix} \frac{1}{3} & 0 & 0 & 0 & 0 & 0 \\ 0 & \frac{13}{35} + \frac{6}{5}\frac{I_y}{S\ell_e} & 0 & 0 & 0 & -\frac{11\ell_e}{210} - \frac{1}{10}\frac{I_y}{S\ell_e} \\ 0 & 0 & \frac{13}{35} + \frac{6}{5}\frac{I_y}{S\ell_e} & 0 & -\frac{11\ell_e}{210} - \frac{1}{10}\frac{I_y}{S\ell_e} & 0 \\ 0 & 0 & 0 & \frac{1}{3}\frac{J}{S} & 0 & 0 \\ 0 & 0 & -\frac{11\ell_e}{210} - \frac{1}{10}\frac{I_y}{S\ell_e} & 0 & \frac{\ell_e^2}{105} + \frac{2}{15}\frac{I_y}{S} & 0 \\ 0 & -\frac{11\ell_e}{210} - \frac{1}{10}\frac{I_y}{S\ell_e} & 0 & 0 & 0 & \frac{\ell_e^2}{105} + \frac{2}{15}\frac{I_y}{S} \end{pmatrix}$$

$$\mathbf{M}_e^{11,s_0} = \rho S \ell_e \begin{pmatrix} \frac{13}{35} + \frac{6}{5}\frac{e^2}{12\ell_e^2} & -\frac{11\ell_e}{210} - \frac{1}{10}\frac{e^2}{12\ell_e} \\ -\frac{11\ell_e}{210} - \frac{1}{10}\frac{e^2}{12\ell_e} & \frac{\ell_e^2}{105} + \frac{2}{15}\frac{e^2}{12} \end{pmatrix} \qquad \mathbf{M}_e^{11,s_1} = \rho S \ell_e \begin{pmatrix} \frac{13}{35}M_{w_1} + \frac{1}{2}\frac{6}{5}\frac{e^2}{12\ell_e^2} & -\frac{11}{210}\ell_e M_{w_1} - \frac{1}{20}\frac{e^2}{12\ell_e} \\ -\frac{11}{210}\ell_e M_{w_1} - \frac{1}{20}\frac{e^2}{12\ell_e} & \frac{\ell_e^2}{105}M_{w_1} + \frac{1}{2}\frac{2}{15}\frac{e^2}{12} \end{pmatrix}$$

$$\mathbf{M}_e^{11,s_i} = \rho S \ell_e \begin{pmatrix} \frac{1}{6} & 0 & 0 \\ 0 & \frac{13}{35}M_{w_i} + \frac{1}{2}\frac{6}{5}\frac{e^2}{12\ell_e^2} & -\frac{11}{210}\ell_e M_{w_i} - \frac{1}{20}\frac{e^2}{12\ell_e} \\ 0 & -\frac{11}{210}\ell_e M_{w_i} - \frac{1}{20}\frac{e^2}{12\ell_e} & \frac{\ell_e^2}{105}M_{w_i} + \frac{1}{2}\frac{2}{15}\frac{e^2}{12} \end{pmatrix} \qquad \mathbf{M}_e^{11,bs_1} = \rho S \ell_e \begin{pmatrix} 0 & 0 \\ 0 & 0 \\ \frac{e^2}{20\ell_e^2} & -\frac{e^2}{240\ell_e} \\ 0 & 0 \\ -\frac{e^2}{240\ell_e} & \frac{e^2}{180} \\ 0 & 0 \end{pmatrix}$$

with $M_{w_1} = (1+2\frac{e^2}{12a^2})$ and for $i \geq 2$ $M_{w_i} = \frac{1}{2}(\frac{i^2+1}{i^2} + \frac{(i^2-1)^2}{i^2}\frac{e^2}{12a^2})$.

The other sub-matrices have similar shapes and terms while the coefficients of $\mathbf{M}_e^{12}$ are different compared to the other two matrices and can be found in the work of [1]. The beam part of the latter reads:

$$\mathbf{M}_e^{12,b} = \rho S\ell_e \begin{pmatrix} \frac{1}{6} & 0 & 0 & 0 & 0 & 0 \\ 0 & \frac{9}{70} - \frac{6}{5}\frac{I_y}{S\ell_e} & 0 & 0 & 0 & -\frac{13\ell_e}{420} + \frac{1}{10}\frac{I_y}{S\ell_e} \\ 0 & 0 & \frac{9}{70} - \frac{6}{5}\frac{I_y}{S\ell_e} & 0 & -\frac{13\ell_e}{420} - \frac{1}{10}\frac{I_y}{S\ell_e} & 0 \\ 0 & 0 & 0 & \frac{1}{6}\frac{J}{S} & 0 & 0 \\ 0 & 0 & -\frac{13\ell_e}{420} + \frac{1}{10}\frac{I_y}{S\ell_e} & 0 & -\frac{\ell_e^2}{140} - \frac{1}{30}\frac{I_y}{S} & 0 \\ 0 & \frac{13\ell_e}{420} - \frac{1}{10}\frac{I_y}{S\ell_e} & 0 & 0 & 0 & -\frac{\ell_e^2}{140} - \frac{1}{30}\frac{I_y}{S} \end{pmatrix}$$

It needs to be noted that $\mathbf{M}_e^{12} = (\mathbf{M}_e^{21})^T$.

Due to the use of an explicit time integration in the resolution of dynamic problems, the consistent mass matrix is replaced by a lumped mass matrix in order to enhance the computational cost of the explicit scheme. The lumped matrix is calculated by the row-sum of the translational terms while the rotational terms are obtained by the scaling of the intertia in the diagonal term. The diagonal blocks of the lumped mass matrix are presented in the following:

$$\tilde{\mathbf{M}}_e^{11} = \tilde{\mathbf{M}}_e^{22} = \rho S\ell_e diag\left(\frac{1}{2}, \frac{1}{2}, \frac{1}{2}, \gamma_b, \gamma_b, \gamma_b, \frac{1}{2}, \gamma_s, \frac{1}{2}, \gamma_s, \frac{1}{2}, \gamma_s, \frac{1}{2}, \frac{1}{2}, (\frac{i^2+1}{i^2} + \frac{(i^2-1)^2}{i^2})\gamma_s\right)$$

The γ coefficients are the rotational terms, which are treated similarly between the beam $\frac{I_y}{S}$ terms and shell $\frac{e^2}{12}$ terms, the i coefficients represent the Fourier mode. It needs to be noted that the three beam rotational terms need to be equal in order to keep the matrix independant of the local or the global basis in the FEM calculations. As a consequence, the torsional term is taken to be equal to the flexural one.

4 Stability condition

The explicit time integration scheme of an undamped system with the central difference operator, requires a stability condition that can be defined as [5]:

$$\Delta t^n = C\Delta t^n_{\text{crit}} \quad \text{with} \quad \Delta t^n_{\text{crit}} = \frac{2}{\omega^n_{\max}} \tag{4}$$

where $0 < C \leq 1$ is the Courant number, Δt^n_{crit} the critical time step and $\omega^n_{\max}$ the maximum eigenvalue of the system which is bounded by the maximum eigenvalue of each element $\omega^n_{e,\max}$:

$$\omega^n_{\max} \geq \max_e \left(\omega^n_{e,\max}\right)$$

The eigenvalue problem of each tube element needs to be solved in order to obtain the maximum value required for the calculation of the time step in equation (4). In contrast to [1] where the natural frequencies of beams (for both axial and flexural beam motions) and cylindrical shells given in [2] are considered, the maximum frequency of each element satisfies $\det(\mathbf{K} - \omega^2\tilde{\mathbf{M}}) = \mathbf{0}$. Obviously, the rotational terms γ_b and γ_s in the lumped mass matrix have an important impact on the value of the eigenvalues and thus on the critical time step.

In this work, the rotational coefficients taken into account are obtained by scaling of the inertia terms for both beam and shell contributions (terms with $\frac{I_y}{S}$ or $\frac{e^2}{12}$):

$$\gamma_b = \frac{\ell_e^2}{105} + \frac{I_y}{S} \text{ and } \gamma_s = \frac{\ell_e^2}{105} + \frac{e^2}{12}$$

5 Results

A case study, previously used in the work of [1] to validate the tube model is chosen. The latter consists on applying a uniform vertical force over a small section of the tube presented in figure 3. The case considered is a clamped tube on both ends with a uniform force applied in the middle for $0.4L < x < 0.6L$ and $\frac{\pi}{2} - \theta_p < \theta < \frac{\pi}{2} + \theta_p$ with $\theta_p = \frac{\pi}{100}$.

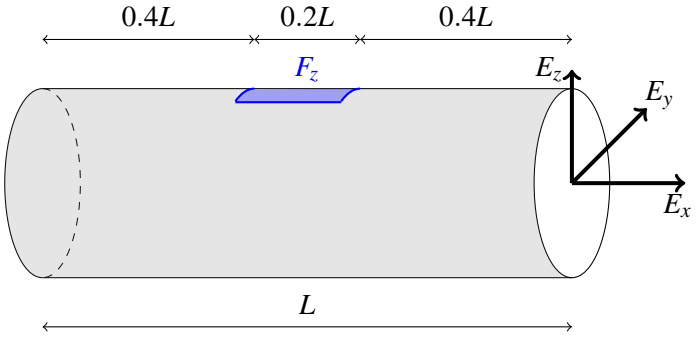

Figure 3: The test case of the tube with the applied uniform force.

First, a mesh convergence study has been conducted over the discretisation of the tube to assess the numerical model. Once the numerical solution is independant of the grid refinement, a stability analysis is performed.

5.1 Mesh convergence

The vertical displacement of the beam contribution V_0 has been computed in the middle of the tube $x = 0.5L$ for all three mesh discretisations with 10, 20 and 40 elements.

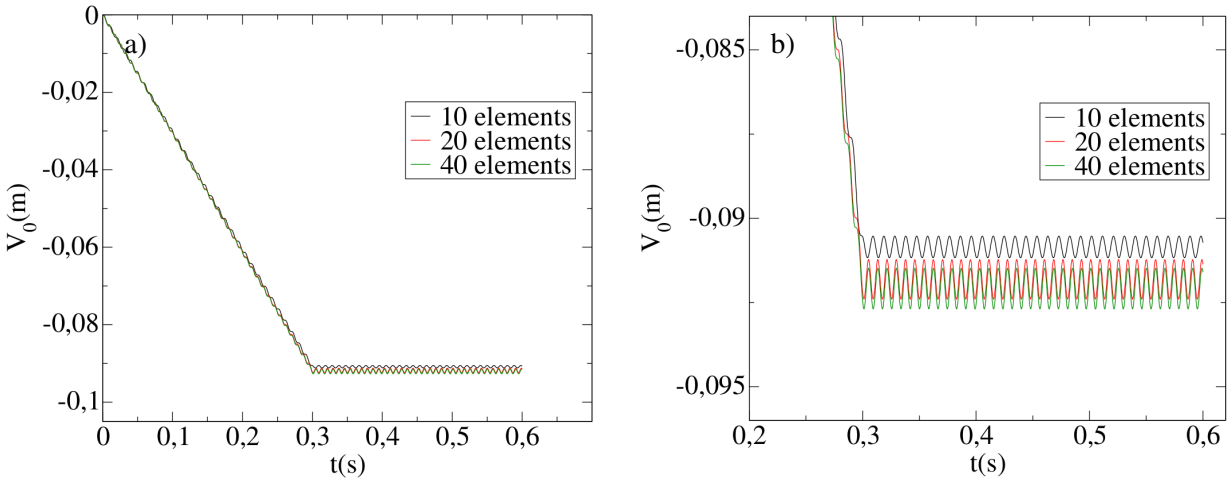

Figure 4: Mesh convergence of the vertical displacement V_0 at $x = 0.5L$: a) the total calculation, b) a zoom over the final stable part.

Figure 4 represents the results of this study for all three meshes. The forces are gradually imposed over time to ensure the numerical stability. A good agreement is observed between the results obtain from the 20 element mesh and the 40 element mesh.

Similar study has been conducted for the cross-section deformation and longitudinal constraint at $x = 0.5L$ presented in figure 5. The latter confirms the agreement between the results obtained by the 20 and 40 element discretisations over the shell degrees of freedom. It can be concluded that given the computational cost and the precision of the 20 element discretisation, it is the reasonable choice for the remaining test.

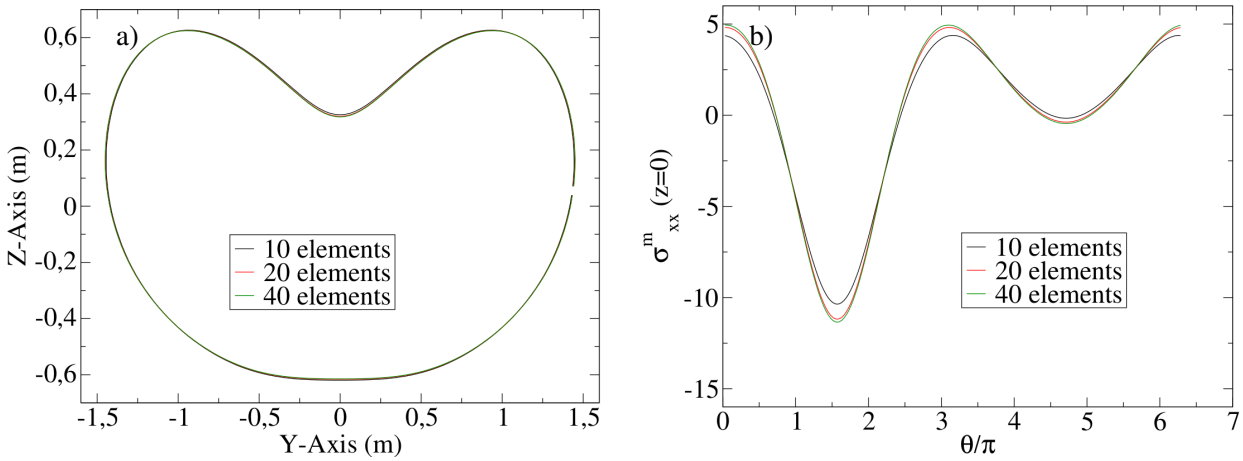

Figure 5: Mesh convergence: a) cross-section deformation and b) longitudinal stress component σ^m_{xx} at $x = 0.5L$.

5.2 Stability analysis

Once the convergence study is conducted, an investigation over the impact of the lumped mass matrix coefficients over the critical time step can be carried out. Using the 20 element discretisation, the time steps of the axial contribution for both beam and shell kinematics, flexural, radial expansion and ovalisation contributions of the tube model are calculated for the considered lumping.

$\Delta t(s)$ axial^b	$\Delta t(s)$ flexural	$\Delta t(s)$ axial^s	$\Delta t(s)$ expansion	$\Delta t(s)$ ovalisation
9.419×10^{-5}	1.864×10^{-5}	1.402×10^{-4}	1.038×10^{-4}	2.276×10^{-4}

Table 1: Time steps corresponding to various tube contributions.

Table 1 sums up all the critical time steps obtained with the lumped mass matrix. It can be observed that the beam flexural time step is smaller than other contributions. On the other hand, the latter depends on the choice of the coefficient of the lumped mass matrix. This coefficient can thus be optimised in order to increase the value of the flexural time step and thus reduce the total computational cost while ensuring an adequate precision of the numerical model. This type of work has been done particularly, in the work of [6] for the beam elements.

6 Conclusion and perspectives

A linear hybrid shell-beam model has been developed in the work of [1] to represent the kinematics of a straight tube. In this work, first the analytical model was explained for both beam and shell kinematics. The numerical model was then presented in which a lumped mass matrix was employed to reduce the computational cost of the explicit time integration. A convergence study of the mesh discretisation was then carried out to furher validate the numerical model. Finally, the stability of the numerical scheme and the minimum time step required for the latter is evaluated for the considered mass matrix lumping.

As observed during the stability analysis, the rotational terms of the lumped mass matrix depend on the γ coefficients of both beam and shell contributions. The latter can be varried in order to optimise the time steps corresponding to each contribution and most importantly, the flexural time step. To increase the accuracy of the enriched beam model, the non-linear coupling terms between the beam and shell contributions need to be taken into account. In order to tackle fluid-structure interaction problems, the present hybrid beam-shell model has to be coupled with a quasi 1D fluid model with varying cross-sections.

Acknowledgments

The first author received a financial support through the project @MECANUM of France Relance. Computational facilities were provided by EDF. Numerical simulations have been performed with the Europlexus software.

References

[1] Pascal-Abdellaoui, Y., Daude, F., Stolz, C., Lafon, P., & Galon, P. *A hybrid shell-beam element for straight thin-walled tubular structures.* Computers & Structures, 285, 107083, 2023.

[2] R. D. Blevins, *Formulas For Dynamics, Acoustics And Vibration.*, Wiley, 2016.

[3] T. von Kármán, *Uber die Formänderung dünnwandiger Rohre*, insbseondere federnder Ausgleichsrohre, Z. Ver. deut. Ing. 55 (1911) 1889– 1895, (in German).

[4] K. Weicker, R. Salahifar, M. Mohareb, *Shell analysis of thin walled pipes. Part I - Field equations and solution*, Int. J. Pres. Ves. & Piping 87 (2010) 402–413.

[5] T. Belytschko, W. K. Liu, B. Moran, K. I. Elkhodary, *Nonlinear Finite Elements for Continua and Structures*, 2d edition, Wiley, 2014.

[6] Belytschko, T., & Mindle, W. L. (1980). *Flexural wave propagation behavior of lumped mass approximations.* Computers & Structures, 12(6), 805-812.